JOURNAL OF MATERIALS SCIENCE 8 (1973) 1218–1232

Deformation of single crystals of gallium arsenide

D. LAISTER*, G. M. JENKINS
Department of Metallurgy, University College of Swansea, UK

Deformation of single crystals of gallium arsenide is reported in bend and tension up to 1000°C whilst maintaining stoichiometry in an arsenic atmosphere. Surface defects and impurity segregation are shown to be dislocation sources. The dislocation density is low enough, however, to show large yield drops which are analysed in detail. Strains of 39% are possible. The activation energy for dislocation movement is increased by heat-treatment owing to an increase in point defect population.

Electron microscopy shows that the predominant slip systems are {111} ⟨110⟩ and the majority of dislocations have $\boldsymbol{b} = a/2$ ⟨110⟩, the axes lying along ⟨110⟩ and ⟨112⟩ directions. Sub-cell formation occurs with sub-boundaries lying along ⟨110⟩ directions.

1. Materials selection

Before any quantitative studies were undertaken on single crystal GaAs, a detailed study of the density and distribution of grown-in dislocations was made in both Czochralski- and gradient freeze-grown ingots. Not only did this provide information concerning deformation occurring during crystal growth, but also enabled a choice to be made as to the most suitable source of single crystal material for deformation studies. The source chosen was gradient freeze-grown GaAs shown in Table I from A down to, and including G; these ingots were comprised of Cr, Zn, Te-doped and undoped GaAs. For the studies made of the effect on the deformation characteristics of various dopants using four-point bending, bar specimens from ingots A, B and C were used. A second series of experiments using samples from these crystals were also carried out after heat-treatment of the specimens at 1029°C for 17 h. It is known that this treatment is sufficient to convert the n-type samples to p-type due to the indiffusion of copper. It was believed that if dislocations were introduced by deformation and were made to move appreciable distances, they would produce sufficient point defects to react with the copper atoms and nullify the effect of the copper by tying it up in Cu-vacancy complexes.

The surface of a specimen could be important

TABLE I Characterization of specimen crystals.

Ingot	Dopant	Hall coefficient R_H(cm³ coulomb⁻¹)		Resistivity ρ (Ω cm)		Mobility (cm² V⁻¹ sec⁻¹)		Carrier concentration N(cm⁻³)	
		Seed end	Tail end	Seed end	Tail end	Seed end	Tail end	Seed end	Tail end
SJC 739	none	415	1260	0.094	0.26	4400	5000	1.5×10^{16}	5.0×10^{15}
SJC 718	Te	26.9	3.51	0.007	0.002	3130	2110	2.32×10^{17}	1.74×10^{18}
SJC 650	Zn	777	127	5.4	0.62	143	204	8.06×10^{15}	4.93×10^{16}
SJC 728	none	200	82	0.05	0.02	4260	3940	3.95×10^{16}	8.82×10^{16}
SJC 680	Cr	Semi-insulating not measured							
SJC 619	Cr								
SJC 725	none	210	131	0.049	0.028	4260	3700	2.98×10^{16}	4.7×10^{16}

*Now at Bell Telephone Laboratories, Ottawa, Canada.

in providing a ready supply of fresh unpinned dislocations for the deformation process and, therefore, an investigation of the nature of surface damage in GaAs was carried out using etching and annealing techniques. Patel and Chaudhuri [1] found a 25% reduction in yield stress during tensile deformation of dislocation-free germanium when specimens had a # 600 SiC grit finish. However, for Ge crystals with a grown-in dislocation density of 10^3 lines cm^{-2}, Bell and Bonfield [2] found that surface preparation had little effect on the yield behaviour. Since it was not known how surface preparation affected the plastic properties of GaAs, four-point bend and tensile tests were carried out on samples with surfaces that had # 600 alumina-lapped finish and others that had chemically polished surfaces.

2. Dislocation distribution in single crystals

Slices that were oriented {1 1 1} and cut from single crystal ingots were etched with the Steinemann [3] etchant to reveal the grown-in dislocations which manifest themselves as triangular pits on the (1 1 1) Ga face where they intersect the surface of the slice. X-ray orientation of the slices using the Laue back-reflection technique using white radiation (W target), enabled crystallographic directions to be assigned to the surface of a slice. These were used for reference purposes. In a sample taken from the impure end of an ingot, there was a fairly random distribution of etch pits near the perimeter of the ingot. This uniform distribution was not translated across a diameter of the crystal and areas were evident where large fluctuations in etch pit density occurred. The overall etch pit density was 1.7×10^4 lines cm^{-2}, whilst that in parts increased to 3.2×10^6 lines cm^{-2}. The sides of the etch pits were parallel to a ⟨1 1 0⟩ direction in the slice. This is the line of intersection of a {1 1 1} plane with the plane of the slice. The apex of a pit was not always symmetrically placed at the centre of the triangular pit and with continued etching the apex moved such as to indicate that the dislocation line was inclined to the slice surface. It was determined by etching that the majority of dislocations lay on the {1 1 1} planes in as-grown GaAs. Electron microscope studies of dislocations in the as-received material showed the majority of dislocations to lie along ⟨1 1 0⟩ directions on {1 1 1} planes with Burgers vector $a/2$ ⟨1 1 0⟩.

Estimates of dislocation densities for GaAs ingots were made by counting the number of pits visible in an area approximately 1 mm^2 and assigning the value to the centre of the area as the density of dislocations at that point. This process was repeated along a number of different diameters in a slice and a mean value obtained for the density at a particular distance along the diameter from the centre of the ingot. There was no difficulty in this method for assessment of Czochralski ingots which were circular in cross-section when grown along the ⟨1 1 1⟩ direction. Gradient freeze ingots had an asymmetrical cross-section and thus it was difficult to obtain a radial distribution representative of a slice in the crystal. The values of dislocation density for such ingots were obtained along the longest axes of the cross-section. The results are shown in Fig. 1. It can be seen that there was less variation in dislocation density for gradient freeze material than Czochralski material. Gradient freeze-grown GaAs was chosen for the deformation studies since this had a more uniform grown-in dislocation distribution and simplified the selection of cleaved specimens from any one slice because of the smaller variation in density across a slice.

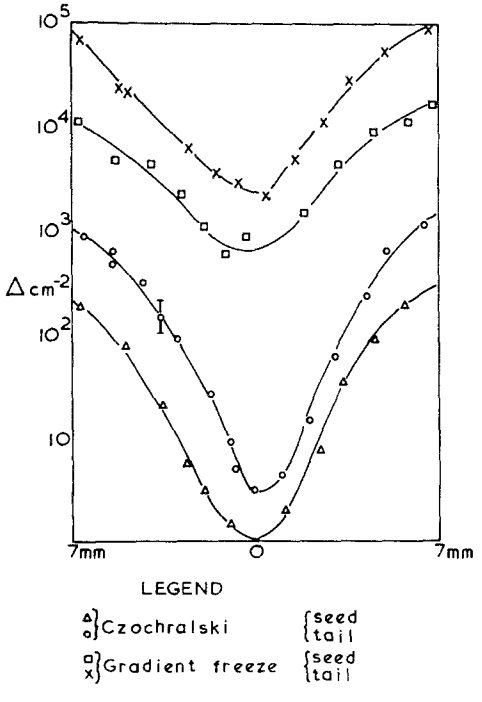

Figure 1 Dislocation density, $\Delta(cm^{-2})$, as a function of the distance from the centre of the ingot along a radius of the crystal.

3. Yield behaviour in the range 500 to 1000°C

The studies made of the deformation behaviour of GaAs below 700°C were carried out using a four-point bending system. For these samples the resolved shear stress σ was calculated from the relationship given by Timoshenko and Goodier [4] and the glide strain, ϵ, from the relationship given by Bruneau and Pratt [5], although these relationships only strictly apply to elastic deformation, the error introduced by extension to the lower yield stress will be small; the errors, however, will become substantial in the region of work hardening. Surface oxidation and loss of arsenic were negligible below 700°C, when using an argon atmosphere. A typical stress-strain curve for GaAs is shown in Fig. 2a. The orientation of the specimens used in the deformation experiments is given in the standard triangle of Fig. 2b. The upper yield point, σ_u, in all samples tested with initial dislocation density $\simeq 10^4$ lines cm^{-2}, occurred in the range 0.3 to 0.5% glide strain. The values of σ_u varied quite considerably for different samples tested under identical conditions. Where the plastic strain-rate of the specimen was again equal to the cross-head velocity of the testing machine, the lower stress, σ_L, varied by less than 10%. Above 700°C deformation was carried out using a tensile apparatus specially designed to preserve stoichiometry (to be described elsewhere). The samples were used subsequently to study the nature and distribution of dislocations in deformed GaAs. The resolved shear stress for tensile specimens was calculated using the relationship given by Barrett [6], and the strain was expressed as the ratio of the increase in specimen gauge length to the original gauge length.

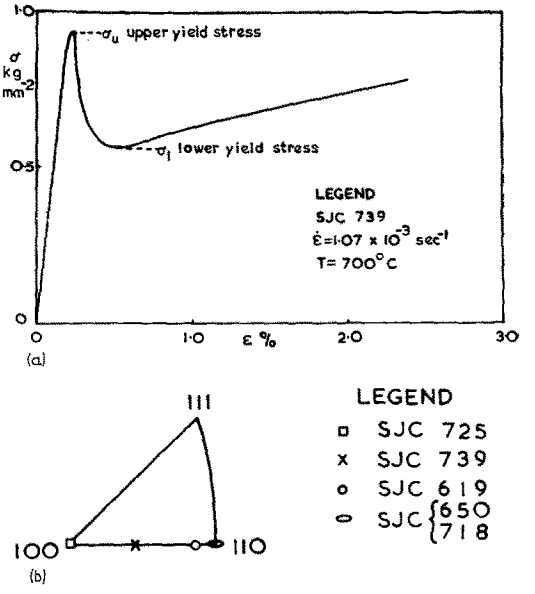

Figure 2 (a) Stress as a function of strain for undoped GaAs produced by four-point bending. (b) Orientation of deformation specimens.

3.1. Effect of surface preparation and pre-strain on the deformation characteristics

With the appropriate choice of strain-rate and temperature, the chemically polished specimens could be made to fracture in a brittle manner, that is before the upper yield stress was reached. Samples of a # 600 alumina-lapped surface under the same conditions deformed plastically. Curve 1, in Fig. 3a, was for a chemically polished sample deformed at 500°C and a strain-rate $\dot{\epsilon} = 2.1 \times 10^{-3}$ sec^{-1}. The results of surface damage and increasing the temperature of deformation on the same material are shown in curves 2 and 3 of Fig. 3a. The increase in temperature of 50°C was more effective in reducing σ_u than was surface damage. Further information on the nature of the yield behaviour was obtained by prestraining the test samples below σ_u, unloading and then immediately retesting. Examination of curves 3 and 4 in Fig. 3b revealed that, not only was the upper yield stress lowered considerably, but also the yield drop was eliminated. The effect of prestrain and surface damage was to increase the density of immediately mobile dislocations available to partake in the deformation. Prestraining was the most effective way of reducing the maximum yield point.

3.2. Etch-pit observations on (111) Ga faces

In the linear portion of the stress-strain curve at the commencement of deformation, slip occurred before the upper yield point was reached and was confined mainly to one slip plane; this was the primary slip plane. At the upper yield point, the total number of dislocation etch pits had increased to 6×10^6 lines cm^{-2}, the dislocation density continued to increase to the lower yield stress whence it remained constant at 10^7 lines cm^{-2}, until slip on a second and third $\{111\}$ $\langle 110 \rangle$ slip system occurred and work-hardening set in. Fig. 4a shows the etch pit arrangement on a (111) face just after the commencement of work-hardening, where three slip systems can be

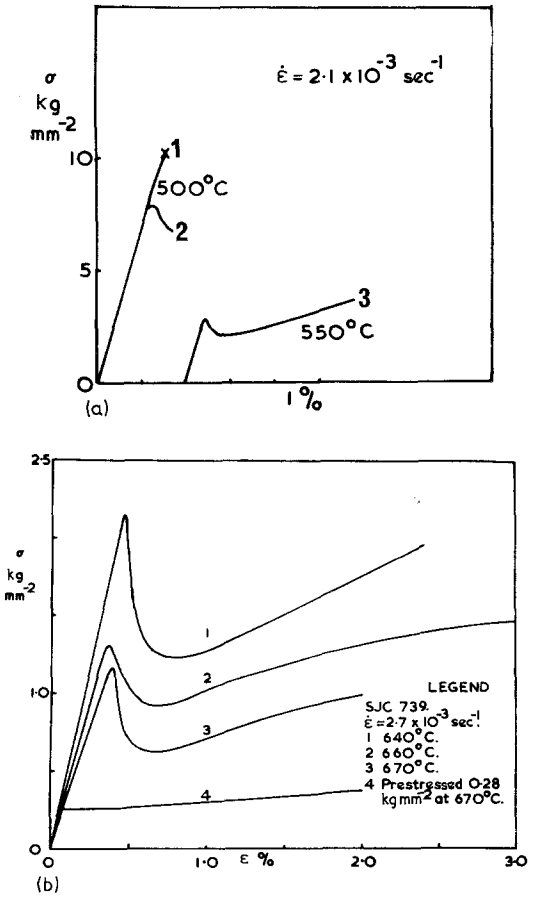

Figure 3 (a) The effect of surface preparation and increase of temperature on stress as a function of strain. (1) Chemically polished surface, (2) # 600 alumina-lapped surface, (3) chemically polished surface. (b) Stress as a function of strain with prestrain and increasing temperature in GaAs.

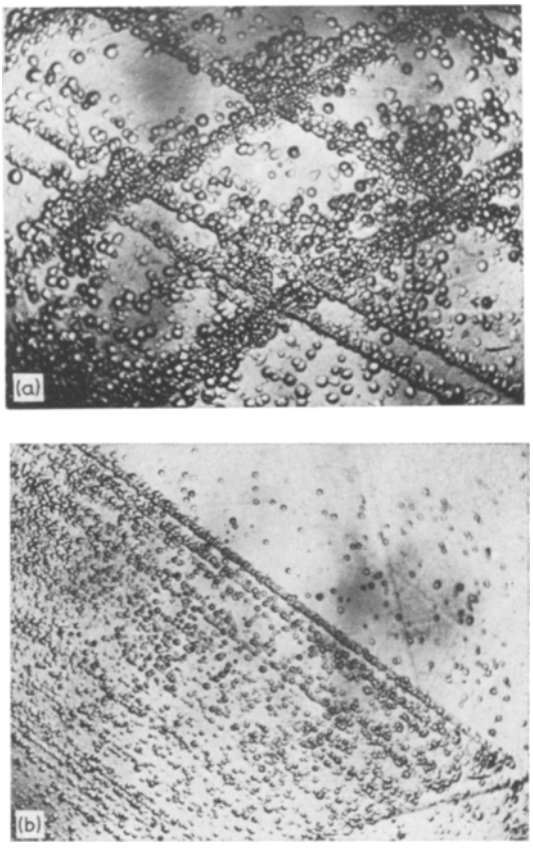

Figure 4 (a) Etch pits on (111) Ga face of a deformed specimen showing slip bands (×385). (b) Dislocation generation in the vicinity of a knife edge during four-point bending (× 257).

seen to be operative. Deformation in the tensile specimens was confined mainly to narrow slip bands, slip having occurred throughout the gauge length by the time the lower yield stress had been reached. In the bending experiments, profuse dislocation generation in the vicinity of the knife edges took place, see Fig. 4b.

3.3. Temperature and strain-rate dependence of the yield stress in GaAs

3.3.1. Non heat-treated GaAs

The temperature-dependence of the lower yield stress, σ_L, (called flow stress by Patel and Freeland [7]) at constant cross-head velocity for undoped Zn and Te-doped GaAs, is shown in Fig. 5a. The straight line relationship on a semi-log plot of stress versus temperature shows that the data are best described by an equation of the form:

$$\sigma_L = A \exp(E_L/kT),$$

where A is some pre-exponential factor and E_L is an activation energy. The values of the various dislocation parameters for non-heat-treated GaAs are contained in Table IIa.

It can be seen from the Table that there was very little difference for the undoped and zinc doped GaAs, whilst Te-doped GaAs was considerably different.

The results show that there will be a yield drop at temperatures up to the melting point of the GaAs, since σ_u and σ_L are not converging. Extrapolation of the curves to 1000°C for a strain-rate $\dot{\epsilon} = 2.7 \times 10^{-3}$ sec^{-1} ,shows that the yield stress should be very small (3.5×10^6 dyn cm^{-2}) for an initial dislocation density of 10^4 lines cm^{-2}. Tests in the region of 1000°C were

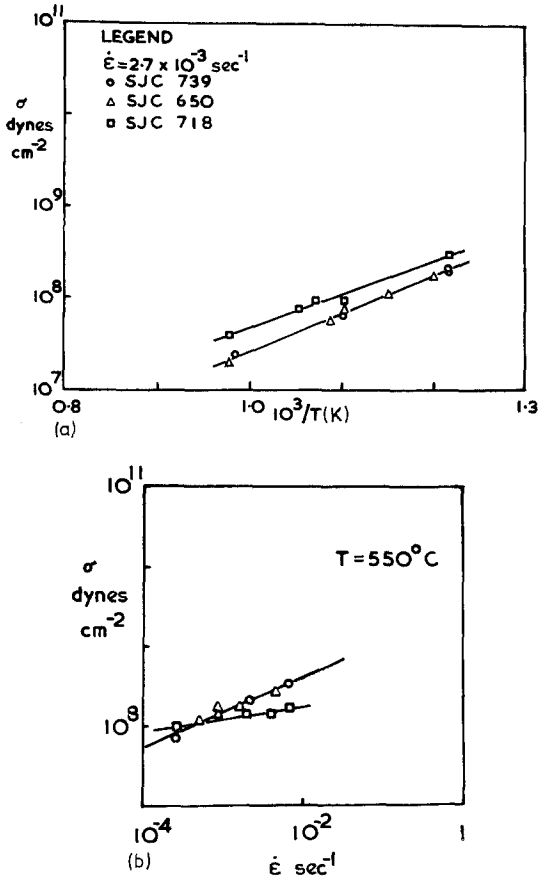

Figure 5 (a) Temperature-dependence of lower yield stress at constant cross-head velocity in undoped, Zn-doped and tellurium-doped crystals. (b) Strain-rate dependence of lower yield stress.

TABLE II a Dislocation parameters for non-heat-treated GaAs.

Ingot	E_L (eV) ± 0.05 (eV)	m ± 0.05	E (eV) ± 0.05 (eV)
SJC 739	1.08	0.422	2.56
SJC 650	1.08	0.422	2.56
SJC 718	0.73	0.175	4.15

TABLE II b Dislocation parameters for heat-treated GaAs.

	E_L (eV) ±0.05 (eV)	m ±0.05	E (eV) ±0.05 (eV)
SJC 739	1.99	0.22	9.05
SJC 650	3.11	0.34	9.11
SJC 718	2.93	0.42	7.03

difficult to assess because the specimens often deformed under their own weight in the tensile jig. For tests successfully carried out at 998°C, there was an extremely small yield stress and yield drop. The stress required to cause dislocation generation and motion in GaAs was very temperature-dependent for all crystals.

The strain-rate dependence of σ_L for GaAs was determined and was found to vary as $(\dot{\epsilon})^m$ as shown in Fig. 5b; the values of the parameter m for the various crystals are given in Table IIa.

The dependence of the lower yield stress on temperature and strain-rate may be understood on the basis of the behaviour of dislocations and their velocities in semiconductors. Because of the nature of the bonding in semiconductors, they have a high Peierls stress for dislocation motion. Haasen [8], Alexander [9] and Chaudhuri *et al* [10] in theoretical arguments, have stated that the velocity, v, of a dislocation should be given by the following relation:

$$v = B\,\sigma \exp\left(-\frac{E}{kT}\right) \tag{1}$$

where σ is the applied shear stress and E is the activation energy for dislocation movement. Patel *et al* [11] found that v was not linear with stress but varied as σ^n. Since the plastic strain-rate is given by:

$$\dot{\epsilon} = N\boldsymbol{b}v \tag{2}$$

where $\boldsymbol{b}$ is the Burgess vector.

Equation 1 becomes:

$$\sigma_L = \left(\frac{\dot{\epsilon}_L}{N_L \boldsymbol{b} B}\right)^{1/n} \exp\left(\frac{E}{nkT}\right) \tag{3}$$

where the subscript L refers to the values of the various parameters at the low yield stress. From this relationship the activation energies for dislocation movement can be obtained using the results contained in Fig. 5a, and b. No conclusions can be drawn concerning the validity of the relationship in Equation 3, since no data are available on actual dislocation velocities in GaAs. However, it is evident that it is more difficult to move dislocations in Te-doped GaAs than in undoped and p-type GaAs, with the carrier concentrations given.

3.3.2. Heat-treated GaAs

The quantitative analysis of the deformation behaviour of heat-treated material is shown in Fig. 6a and b and the corresponding dislocation parameters are given in Table IIb. The activation energies of the undoped and zinc-doped GaAs are still virtually the same, whilst that of pure GaAs is lower, showing that dislocation motion is relatively more easy in these crystals. The over-

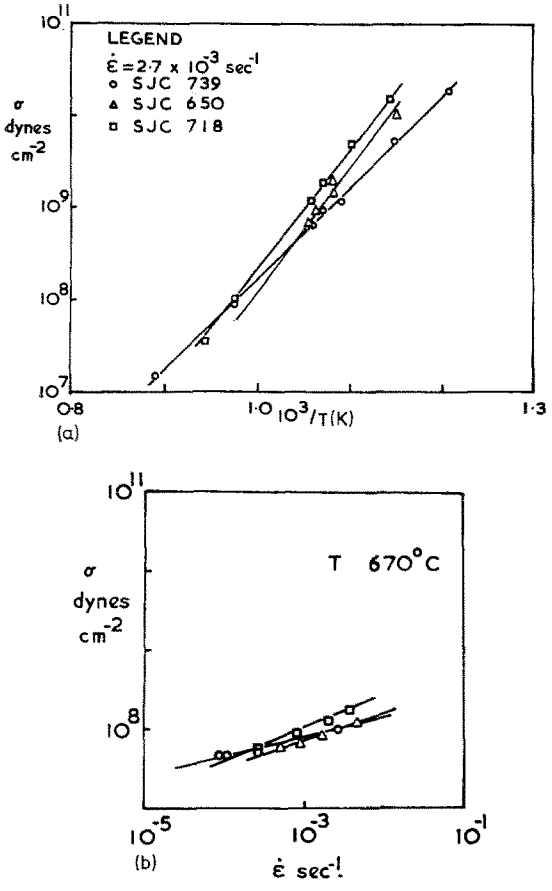

Figure 6 (a) Temperature-dependence of lower yield stress at constant cross-head velocity in heat-treated crystals. (b) Strain-rate dependence of the lower yield stress for heat-treated GaAs.

all activation energies are higher than those of non-heat-treated GaAs.

4. Distribution and nature of dislocations in deformed GaAs

4.1. Deformation processes

The specimens were taken from either undoped or chromium-doped ingots with characteristics shown in Table I. The chomium-doped GaAs was high resistance semi-insulating single crystal. The specimens were tested in the temperature range 750 to 998°C at strain-rates between 6×10^{-5} to 1.5×10^{-2} sec^{-1}. The tests were terminated at various stages in the deformation cycle, samples being taken at points just before the upper and lower yield stresses, also during the linear portion of work-hardening (equivalent to stage II in fcc metals) and finally during the regions of decreasing stress (stage III in fcc metals), and at the termination of stage III where the specimen fractured. The orientation of the samples SJC 680, 728, 619 and 725 are given in Fig. 2b. In specimens oriented with the plane of the electron microscope foil parallel to the broad surface of the I-shaped tensile specimen, {100}, and with tensile axis ⟨100⟩, it was not possible to index the axis of loading uniquely in the micrographs because of the symmetry of the orientation chosen. In specimens SJC 725 that had a {110} plane parallel to the broad surface of the I-shaped specimen and tensile axis ⟨100⟩, the tensile axis of loading could be indexed; this was parallel to the 004 **g** vector. Specimens oriented with the tensile axis along ⟨100⟩ had four slip systems available for operation, except SJC 619 oriented near ⟨110⟩ which had only two systems.

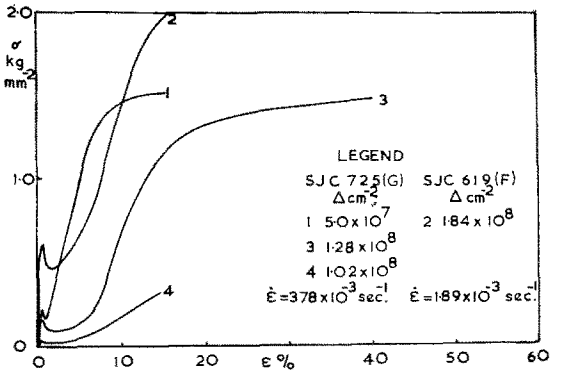

Figure 7 Stress/strain for undoped and chromium-doped GaAs deformed in tension, at $T = 850$°C; Δ: final dislocation density.

Typical stress-strain curves obtained during the tensile deformation of GaAs for chromium-doped and undoped GaAs, are shown in Fig. 7. These were for tests carried out at 850°C and, as can be seen from the curves of samples from ingot SJC 725, the deformation behaviour of the different specimens was quite varied for identical deformation conditions. This was not really surprising since even in gradient freeze-grown GaAs, there was a variation in dislocation density across a diameter of a slice of at least one order of magnitude and because of size limitations only one I-section specimen could be cut from one slice of an ingot oriented ⟨100⟩ or ⟨110⟩. Slip usually occurred first in the vicinity of the grips of the tensile jig at the ends of the gauge length; here the initial dislocation density was usually higher than at the centre of the gauge length as

shown previously in the data on the density and distribution of dislocations in as-grown ingots and thus slip would be expected to occur first in these regions. Although the maximum strain-to-fracture at this temperature was usually in the region of 14 to 16%, occasionally strains such as that for curve 3 in Fig. 7 were recorded. One specimen from ingot SJC 619, under similar conditions to those of the sample represented by curve 2 in Fig. 7, had a strain-to-fracture of 33% and an overall final dislocation density, Δ, of 2.14×10^8 cm^{-2}.

The specimens that fractured at $\sim 15\%$ strain, had final overall dislocation densities, Δ, that were lower than the specimens that fractured after much higher strains. Fracture of the tensile specimens in GaAs occurred, usually, within the gauge length away from the jaws of the jig. The specimens that exhibited the equivalent of a stage II hardening in fcc metals had a work-hardening coefficient

$$\frac{d\sigma}{d\epsilon} = 2.0 \times 10^7 \text{ dyn cm}^{-2},$$

which was approximately independent of temperature. In curves 1 and 2 there was no equivalent of stage I hardening, while curves 3 and 4 show quite an extensive stage I. Stage II was absent in 4 and stage I immediately preceded stage III. The final dislocation densities of 3 and 4 were almost identical, yet 3 had received 26% more strain.

4.2. Dislocation distribution

A comparison was made of the dislocation densities, Δ, determined by electron microscopy with those from etching techniques. The samples for etch-pit examination were the pieces that remained from the gauge length, after machining of the disc specimens for electron microscopy. Table III gives the results of these determinations.

For dislocation densities greater than 10^5 lines cm^{-2}, the correlation between the two methods of determination was good. At low densities, there was a discrepancy between the two methods because electron microscopy tends to lead to over-estimates of the values of Δ, since the areas available for examination are much smaller than in the etch-pit determination.

The region in the pre-lower yield stress portion of the stress-strain curve was characterized by an increasing dislocation density, the dislocations being mainly confined to the one slip plane. Some dislocation movement was taking place on other slip planes as can be seen in Fig. 8a which was taken of a sample of semi-insulating GaAs deformed at 750°C at a strain-rate of $\dot{\epsilon} = 1.89 \times 10^{-3}$ sec^{-1}. At the lower yield stress and in the portion of the curves representing easy glide, when this was exhibited by a specimen, the substructure was characterized by dislocations lying along $\langle 1\,1\,0 \rangle$ directions in the foil. At this stage, dislocation lines on slip planes other than the primary plane, had intersected those of the primary system, as can be seen in Fig. 8b which was for undoped GaAs deformed at 800°C and $\epsilon = 1.89 \times 10^{-3}$ sec^{-1}. The contrast effects seen between the loops were similar to those seen by Low and Turkalo [12] in silicon iron. This contrast between the dislocation and the surrounding matrix indicates that the foil was highly strained in this region. These dislocations lay on parallel $\{1\,1\,1\}$ slip planes but none were found arranged in pile ups. At this stage of the deformation cycle a large number of dislocation

TABLE III Dislocation densities, Δ, determined for tensile specimens using etch-pit and electron microscopy.

Specimen	Dislocation density, Δ (cm^{-2})			
	As-received		Deformed	
	Etch-pit	Electron-microscopy	Etch-pit	Electron-microscopy
SJC 680 (1)	3.17×10^4	4.30×10^4	7.58×10^7	7.9×10^7
SJC 680 (2)	9.12×10^3	2.4×10^4	6.00×10^7	6.25×10^7
SJC 680 (3)	9.92×10^4	1.03×10^5	4.86×10^7	4.97×10^7
SJC 728 (1)	6.74×10^4	6.9×10^4	2.5×10^6	2.0×10^6
SJC 728 (2)	6.74×10^4	7.3×10^4	9.83×10^7	1.01×10^8
SJC 785 (1)	8.92×10^4	9.49×10^4	1.05×10^8	1.02×10^8
SJC 785 (2)	3.80×10^4	4.01×10^4	1.09×10^8	1.08×10^8
SJC 785 (3)	1.02×10^4	3.85×10^3	8.07×10^7	5.0×10^7

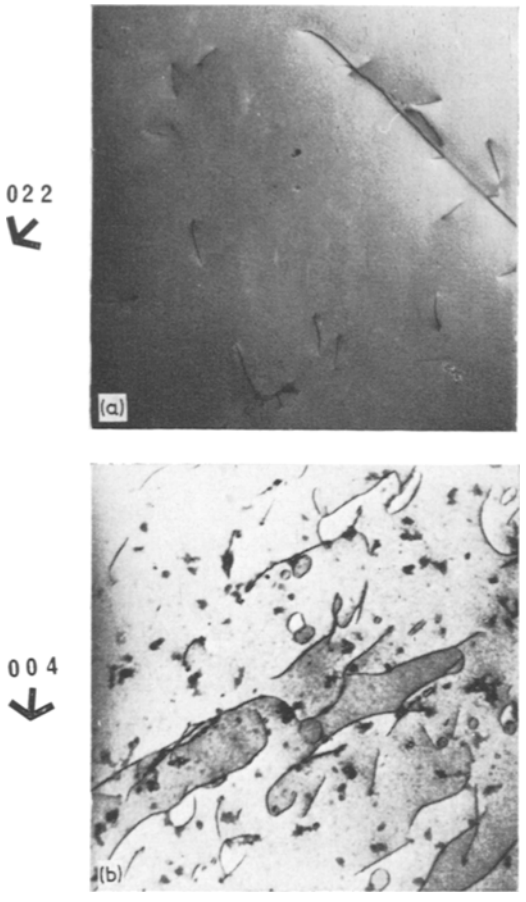

Figure 8 (a) Bright field TEM of semi-insulating GaAs deformed at 750° C after 0.2% strain: g = 022 (× 18700) (b) Bright field TEM of undoped GaAs deformed at 800° C after 0.8% strain: g = 004 (× 11700).

loops were found associated with the dislocation bands. As shown in Fig. 9a, these were either circular or elongated. It is believed that the circular loops were formed by the pinching-off of elongated loops and their subsequent growth occurred by capture of point defects created by non-conservative dislocation movement within a band. This process of pinching-off can be seen in Fig. 9b where a loop is seen in the process of being separated.

At the commencement of stage II deformation, there was a rapid development of a highly disordered dislocation structure as shown in Fig. 10a. Here, the long axes of the dislocations lay parallel to the ⟨220⟩ and ⟨400⟩ directions in the foil and shorter segments along ⟨210⟩ directions; these data are consistent with dislocations lying along ⟨110⟩ and ⟨112⟩ directions on the {111} slip planes. The highly disordered dislocation arrangement preceded the formation of dislocation walls, (Fig. 10b), the interior of the cell structure, thus formed, becoming relatively free of dislocations. In the early stages of sub-boundary formation, it was still possible to distinguish the slip systems. The dislocation sub-boundaries tended to lie along the ⟨110⟩ directions in the foil; these were the lines of intersection of the {111} planes which contained the majority of slip dislocations.

In the final stage of deformation, stage III, sub-boundary formation became quite pronounced and the misorientations across sub-boundaries became measurable. This was done using the method employing the shift of Kikuchi bands in selected-area diffraction patterns. Since rotation of a foil causes the Kikuchi lines in a diffraction pattern to shift as though they were rigidly

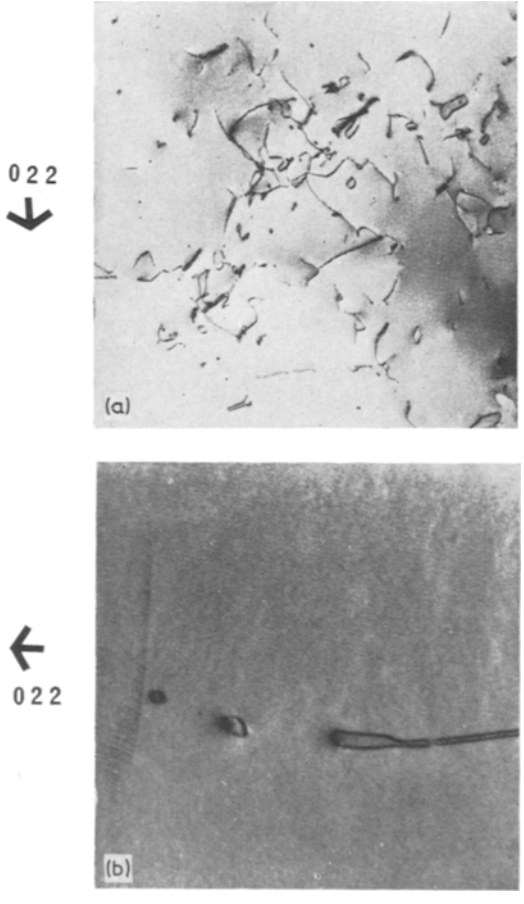

Figure 9 (a) Dislocations, showing slip bands developing: g = 022 (× 11800). (b) Dislocation trail left by dipole pinching-off: g = 022 (× 45000).

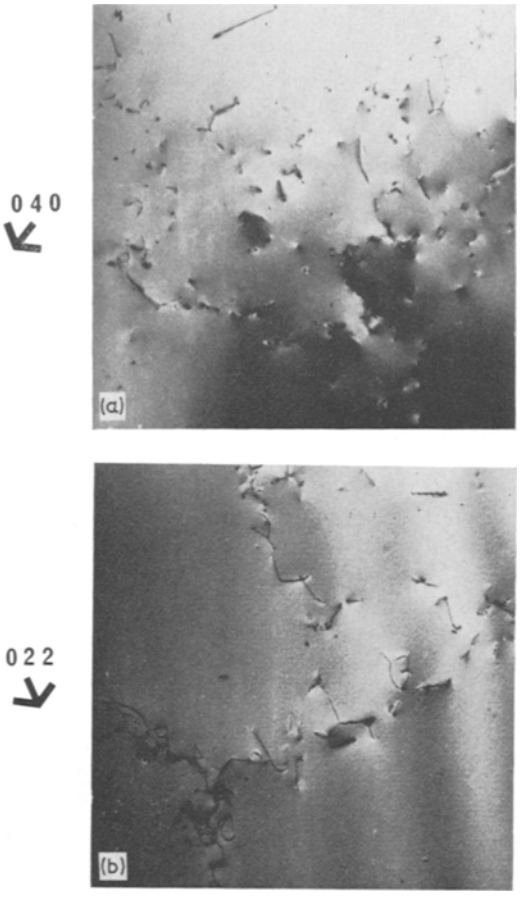

Figure 10 (a) Dislocation at commencement of stage II hardening: $\mathbf{g} = 040$ (× 11800). (b) Dislocation walls: $\mathbf{g} = 022$ (× 11800).

attached to the foils, estimates, to within 0.1 degree, for orientation determination were possible (Hirsch *et al* [13]). Fig. 11a and b show two such boundaries, the boundary in Fig. 11a has a misorientation of ~ 0°6′ and that in Fig. 11b, ~ 0° 17′. The corresponding diffraction conditions to Fig. 11a and b are contained in Fig. 11c and d. During stage III, the whole crystal was in a state of flux and new boundaries were continually forming, as shown in Fig. 12. Here there are a larger number of smaller dislocation loops than when sub-boundaries formed during the start of stage II, and there are also a greater number of dislocation dipoles. Thus, Fig. 12b is an enlargement of part of the area shown in Fig. 12a, so that the dipole configuration can more easily be seen; note the dislocation marked A, B, C, D, which contains a complex loop configuration at these points. In specimens that had undergone more than 15% strain, the sub-boundaries became more complex and hexagonal dislocation grids were seen. For example, in Fig. 13a, the short lengths of dislocation lay along the ⟨111⟩, ⟨210⟩ and ⟨400⟩ directions, as did the majority of sub-boundaries. Initially sub-boundaries were aligned along ⟨111⟩ directions in these specimens, but, as can be seen in Fig. 13b, boundaries also formed along (220) directions after the commencement of stage II. At the later stages during stage III hardening, the misorientation across sub-boundaries increased. Note the contrast difference between dislocation tangles in Fig. 14a and across the single boundary in Fig. 14b. The sample deformed to 40% strain had become polycrystalline.

In the highly disordered dislocation tangles and networks at the sub-boundaries, some dislocation rearrangement was seen taking place in the electron microscope as heating took place in the electron beam. This rearrangement was confined to isolated dislocation segments in a network. In no circumstances were any dissociated dislocations seen in deformed GaAs; from this observation and the dislocation arrangement (Howie [14]), it is construed that the stacking fault energy for GaAs is in the medium to high range.

4.3. Nature of dislocations in GaAs

The $\mathbf{g} \cdot \boldsymbol{b} = 0$ criterion was obtained by tilting a foil containing dislocations introduced by deformation on a high-tilt cartridge goniometer stage.

Fig. 15a to d are micrographs of an area in a [110]-oriented foil and the resulting dislocation contrast seen for the foils examined in the reflections $\mathbf{g} = \bar{2}22$, $\bar{2}20$, $\bar{2}2\bar{2}$, $1\bar{1}3$. In the reflections where $\mathbf{g} \cdot \boldsymbol{b} = 0$ for a particular dislocation, there was still some residual contrast due to the edge character of the dislocations. Dislocations were aligned along the ⟨220⟩, ⟨222⟩ and ⟨400⟩ directions in the foil. Those aligned along ⟨400⟩ were inclined to the surface of a foil as were some of those lying along ⟨222⟩ directions. Combined with the information obtained from [100] oriented foils, the axes of dislocations were identified as ⟨112⟩ and ⟨110⟩. Analysis of the dislocation segments A, B, C and D in Fig. 15b will be dealt with in detail.

The dislocation contrast effects are summarized in Table IV, where I and V represent

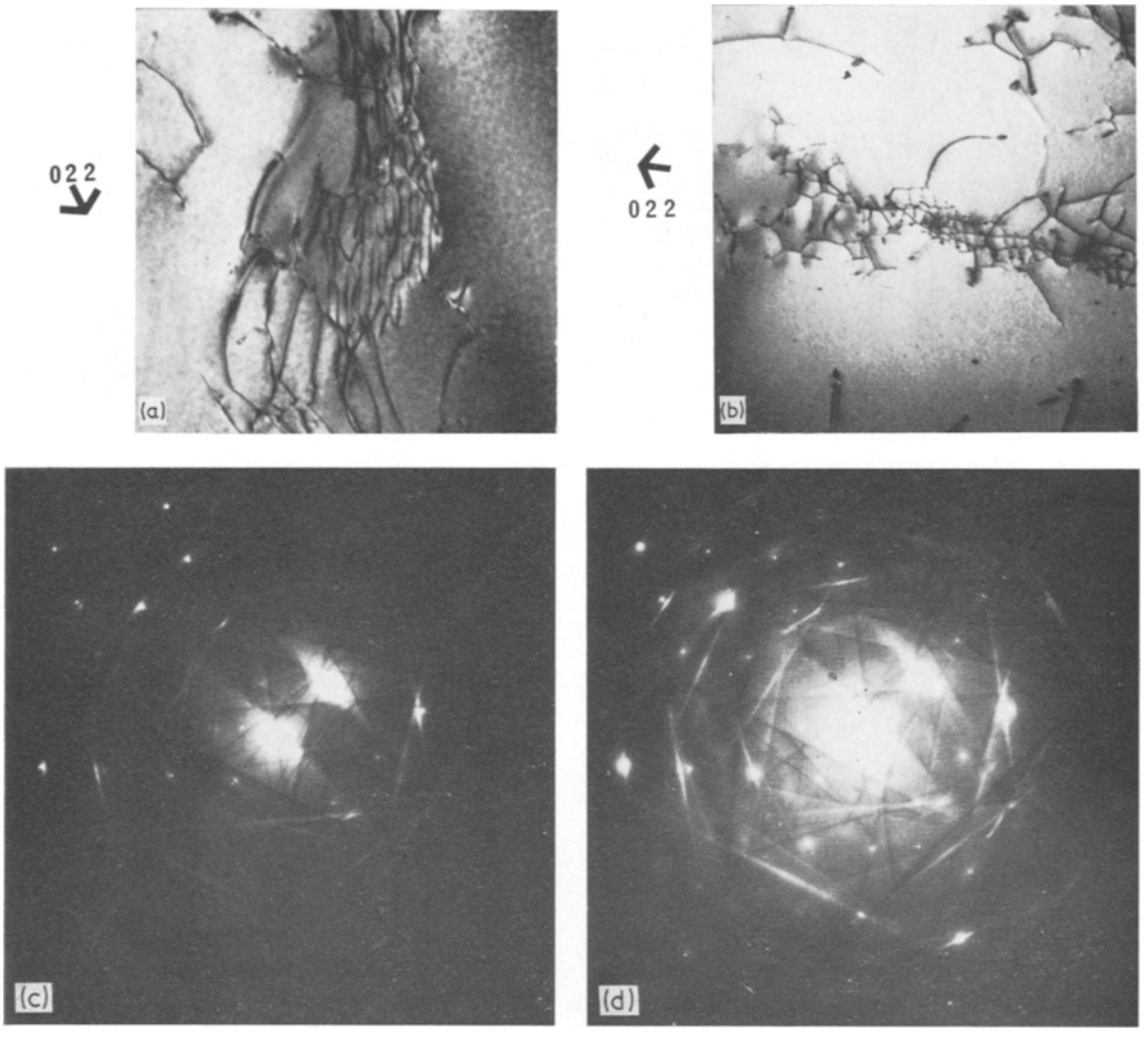

Figure 11 (a) Sub-boundary in Cr-doped crystal deformed 16%: $\mathbf{g} = 022$ (× 58000). (b) As (a) (× 23000). (c) SADP from Fig. 11a ($\xi_g \bar{S}g = 0$). (d) SADP from Fig. 11b ($\xi_g \bar{S}g > 0$).

invisibility and visibility respectively. From this, the possible Burgers vectors were found to be for A and B,

$$\boldsymbol{b} = \pm \tfrac{1}{2}[101]$$

and for C and D,

$$\boldsymbol{b} = \pm \tfrac{1}{2}[011].$$

The ambiguity of $\boldsymbol{b}$ was resolved by examining the dislocations in 242 reflections about the [210] normal, 18.4° away from the [110] normal along the 004 Kikuchi band. When $\mathbf{g} = 242$, A, D and B were visible but C was invisible; therefore, $\boldsymbol{b}_C = \pm \tfrac{1}{2}[101]$. When $\mathbf{g} = \bar{2}42$, A and D were invisible; therefore, $\boldsymbol{b}_{A,D} = \tfrac{1}{2}[101]$. The axis of C was along a 112 direction with $\boldsymbol{b}_C = \pm \tfrac{1}{2}[101]$. From the sense of inclination of C by tilt about the ⟨220⟩ axis, the habit plane of this segment of dislocation was determined as (111). Thus, the dislocation corresponds to type IV in the Hornstra [15] notation.

TABLE IV Contrast of dislocations in Fig. 15 for reflections g in a [110] oriented foil.

Dislocation	g			
	$\bar{2}22$	$\bar{2}20$	$\bar{2}2\bar{2}$	$1\bar{1}3$
A	I	V	V	V
B	V	V	I	V
C	V	V	I	V
D	I	V	V	V

In sub-boundaries, dislocation segments had

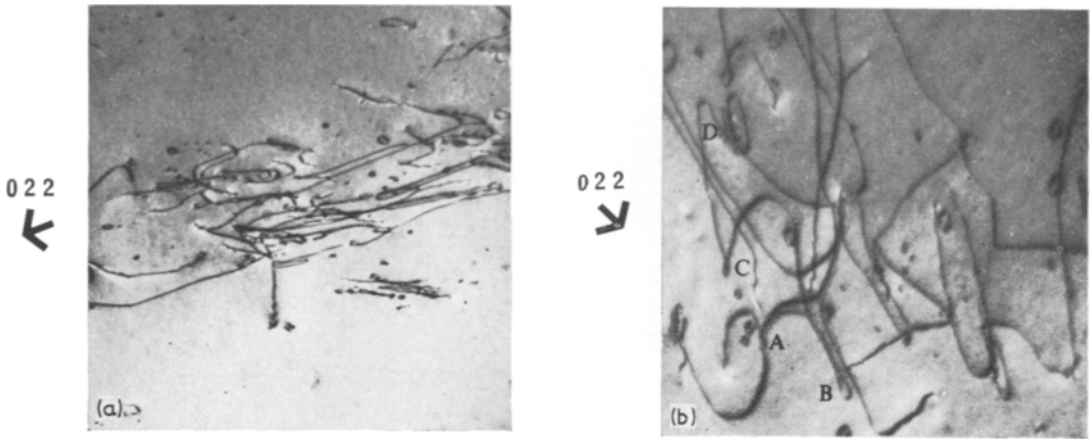

Figure 12 (a) Dislocation boundary in deformed GaAs showing large number of loops: g = 022 (× 23000). (b) Detail of 12a: g = 022 (× 59000).

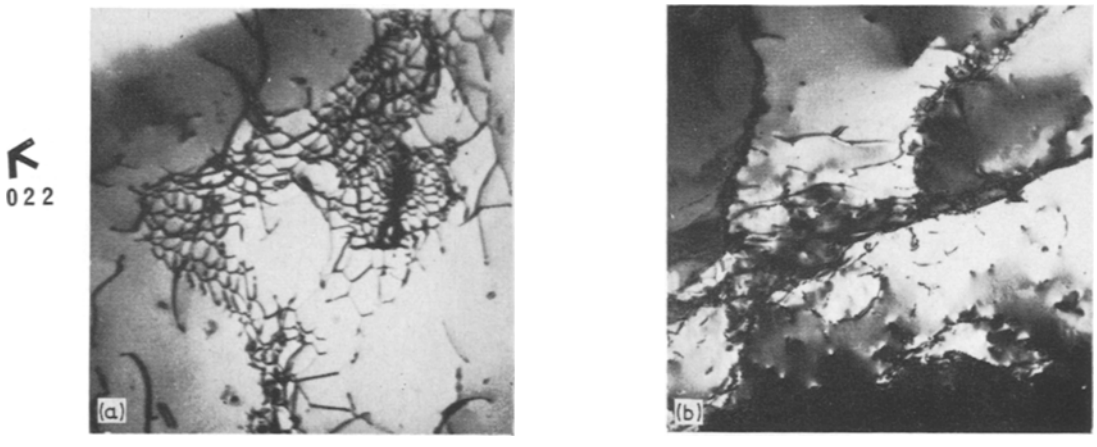

Figure 13 (a) Networks in undoped crystal deformed 39%: g = 022 (× 58000). (b) Dislocation cell walls (× 9300).

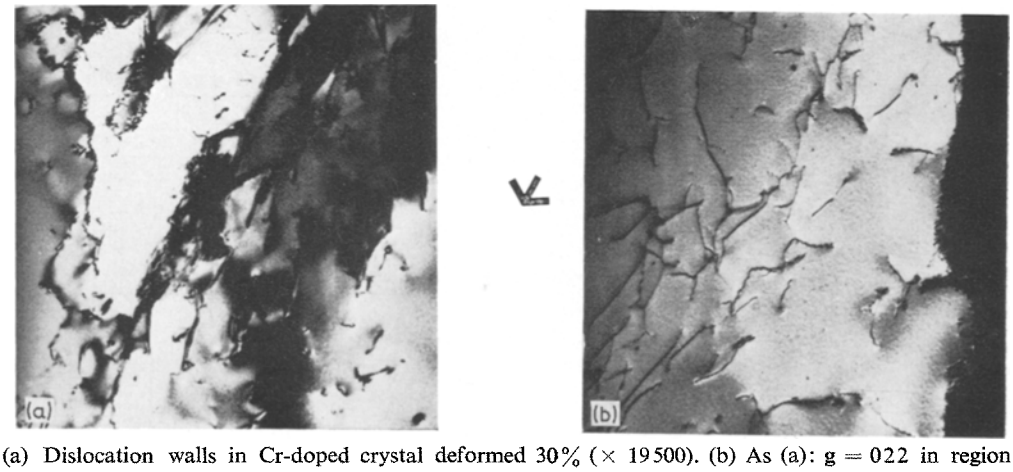

Figure 14 (a) Dislocation walls in Cr-doped crystal deformed 30% (× 19500). (b) As (a): g = 022 in region showing light contrast.

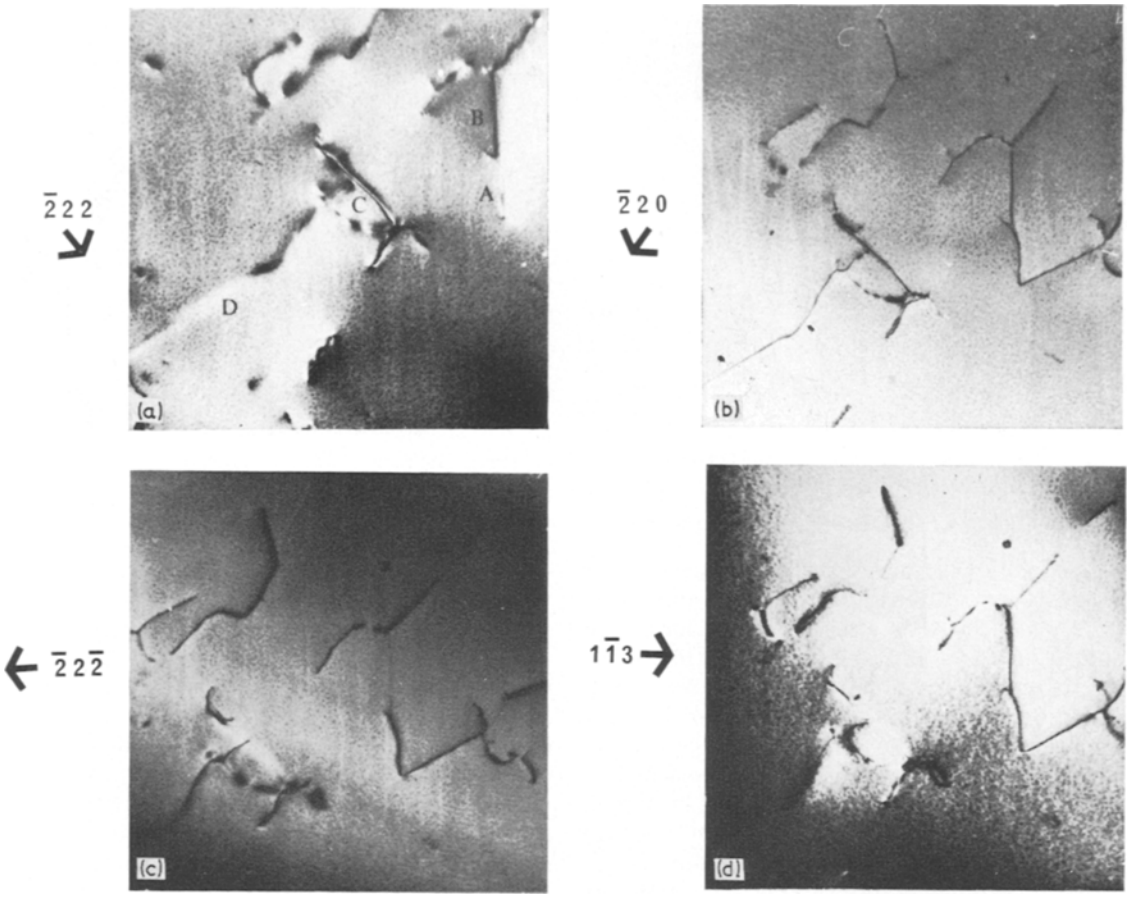

Figure 15 (a) Dislocations in a [110] oriented, deformed GaAs foil: $\mathbf{g} = \bar{2}22$ (× 24500). (b) As (a): $\mathbf{g} = \bar{2}20$ (× 24500). (c) As (a): $\mathbf{g} = \bar{2}2\bar{2}$ (× 24500). (d) As (a): $\mathbf{g} = 1\bar{1}3$ (× 24500).

their major axes along ⟨111⟩ and ⟨220⟩ directions while the shorter connecting segments lay along the ⟨400⟩ directions in ⟨110⟩ oriented foils, as can be seen in Fig. 16a. Here the segments along ⟨220⟩ show only residual contrast and so $\boldsymbol{b} = \pm\frac{1}{2}[110]$. Fig. 16b shows a boundary arrangement in a [100]-oriented foil, the dislocation segments were aligned along ⟨220⟩ for the majority of dislocations while short segments lay along ⟨400⟩ and ⟨210⟩ directions.

5. Discussion

5.1. Effect of defects and dopants on yield behaviour

Yield drop phenomena in non-metallic crystals has been extensively discussed by Johnson and Gilman [16] and in an extended treatment of this phenomenon, Cottrell [17] has given the following criteria for discontinuous yielding:

(a) the total dislocation density $\Delta = 0$ and stress concentrations should be small, or:
(b) the number of mobile dislocations per unit volume of crystal $L_M = 0$ and $\Delta = 0$, or:
(c) L_M should be greater than 0 and the glide stress, σ, sensitive to the velocity of the dislocation.

In most semiconductor materials, condition (c) is the one responsible for the yield drop. In the tests on GaAs studying the effects of prestrain and surface preparation, the lowering of the yield stress, σ_M, is due to the increase in the number of mobile dislocations. These need to move slower at a given strain-rate to accommodate the applied strain-rate compared to smaller numbers, and therefore require a lower stress. The necessary condition of a supply of fresh dislocation for plastic deformation to take place at very high strain-rates and low tempera-

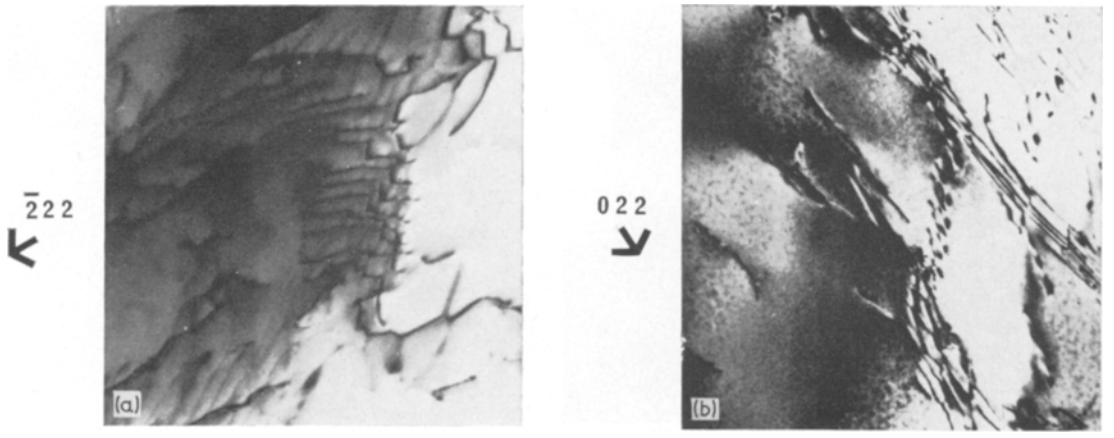

Figure 16 (a) Dislocation network in [110] GaAs foil deformed 39%. $\mathbf{g} = \bar{2}22$ (× 36500). (b) Dislocation network in [100] GaAs foil deformed 30%. $\mathbf{g} = 022$ (× 24300).

ture conditions shown for GaAs suggests that grown-in dislocations are pinned in some way. It seems likely that although dislocations are pinned in GaAs and that condition (b) will be operative at the commencement of a test, condition (c) is the one responsible for the yield drop, since dislocation movement and generation occurs before the upper yield stress is reached.

Analysis of the results on the effect of doping on the plastic behaviour of GaAs, must take into account the elastic and electrical interactions between the moving dislocations and impurities and point defects of the host lattice, together with the possible structure of the dislocations and the influence of impurities on the concentration of point defects. Consequently, interpretation is difficult. The activation energy for dislocation movement in Te-doped GaAs is higher than for either Zn-doped or undoped material. This is at variance with the results of Sazhin *et al* [18] which indicate that Zn-doped crystals are more easily deformed than either Te-doped or undoped crystals. Electron microscopy of annealed samples suggests that point defect concentration in Te-doped GaAs increases with increasing Te concentration and that Te-doping produces a higher proportion of point defects than is present in undoped crystals. Therefore, the higher activation energy for Te could be explained by point defect-dislocation interaction. During dislocation motion, the strain field of the dislocation can interact with the strain field of a vacancy and thus influence dislocation mobility. The higher activation energies for the heat-treated samples could be related to a vacancy mechanism, since heat-treatment in the presence of copper would tend to increase the concentration of vacancies during its indiffusion. The lower value for Te-doped GaAs would be ascribed to the greater extent of annealing of point defects owing to a higher copper concentration, as postulated for the different rates of loop annealing [19]. Alternatively, dislocation motion could be restricted due to the presence of jogged segments of dislocation. Dash [20] has shown that the motion of screws in silicon can be restricted by the formation of defect trails left in their wake. In our electron microscope examination of GaAs, dislocations were seen to be locally restricted and dipole formation was a common occurrence. However, Chaudhuri *et al* [10] have found that there is a negligible stress-dependence of dislocation velocity, so that the spacings of jogs must be of the order of a few Burgers vectors. Hornstra [15] considered dislocations in these types of crystals to be built up of jogged segments and thus deformation should produce large point defect populations. In thin foils of deformed GaAs, prismatic loops are readily in evidence [19], indicating that a large point defect population exists in the deformed crystal. Celli *et al* [21] considered the motion of dislocations to be restricted by barriers along the dislocation length in the form of pinning points; such points may be jogs, vacancies or impurity atoms. In the few cases of dislocation movement observed by us in the electron microscope in GaAs, where the motion was quite slow due to the low temperature and the high Peierls resistance of the lattice,

movement occurred by a rippling motion along the length of the dislocation. Condensation of impurities and/or vacancies, will lead to non-conservative motion of screw and mixed dislocations and consequently dislocation motion will be dependent upon the defect population of the crystal.

It is not possible, therefore, to draw any definite conclusions concerning the effect of dopants on dislocation kinetics in GaAs, except that increasing the doping level of Te in GaAs causes flow to occur at higher stresses.

5.2. Stresses created by the indiffusion of dopants in GaAs

During diffusion cycles, the relative strain-rate of deformation imposed upon the GaAs slice by the diffusing element is likely to be extremely low and thus the results obtained for the yield stress in GaAs in the strain-rate range 10^{-4} to 10^{-2} sec^{-1} for an initial dislocation density of 10^4 cm^{-2}, are on the high side for comparable material used in device production. For the comparatively high strain-rate of $\dot{\epsilon} = 2.7 \times 10^{-3}$ sec^{-1} in Te-doped GaAs with $N = 10^{18}$ cm^{-3}, extrapolation of the data to the melting point shows that a decrease in the lower yield stress to $\sim 10^6$ dyn cm^{-2} occurs. Using the data given by Black and Lublin [22] for the maximum possible induced stress caused by the indiffusion of zinc in GaAs, σ_{max} is 4.4×10^7 dyn cm^{-2}. Therefore, profuse dislocation generation will occur in Te-doped GaAs when diffused with zinc under the above conditions at temperatures in excess of 10^3 K. However, because of the relatively slow rates of deformation during diffusion of slices,dislocation generation is likely to occur at much lower stresses than in the example given.

5.3. Substructure of the deformed sphalerite lattice of GaAs

The deformed substructure of GaAs in the samples examined, is characterized by the presence of numerous dislocation dipoles, elongated and contracted dislocation loops and, as shown in Fig. 9b, pinching-off of dipoles, producing such loops. It is believed that the cause of dislocation multiplication and generation is the cross-slip of screw segments of the dislocations giving rise to large jogs. Since jogs cannot glide, long narrow cusps consisting of dipoles are formed and if the screws cross-slip back to the original glide plane, or localized diffusion takes place, an elongated loop is formed. Repetition of this process leads to the situation observed in Fig. 9b. Growth of the jog to macroscopic dimensions allows the two arms of the cusp to pass each other and thus leads to multiplication. The random fracture characteristics may be due to the chance development of microcracks associated with the coalescence of Lomer dislocations, as proposed by Abrahams and Ekstrom [23] to explain cleavage in GaAs; failure almost invariably occurred on {1 1 0} planes. Although examples of Lomer reactions were not detected in GaAs, these reactions have been seen in other semiconductors, notably silicon (Jenkinson and Lang [24]).

6. Conclusions

(a) Dislocations in as-grown crystals have an overall density higher in gradient freeze ingots than in Czochralski ingots.

(b) GaAs exhibits yield phenomena similar to other semiconductor type crystals. Te-doping produces material with a higher yield stress than comparable samples of undoped and Zn-doped crystals and a yield drop is expected to occur up to the melting point. Heat-treated GaAs shows unusual yield behaviour; the activation energy for dislocation movement is higher than in non-heat-treated material and is probably due to an increase in the point defect population. Te-doped GaAs now has the lower activation energy. Pre-yield deformation produces the most significant drop in yield stress and surface source of dislocations only become important under extreme deformation conditions.

(c) The predominant slip systems in GaAs are {1 1 1} ⟨1 1 0⟩ and the majority of dislocations have Burgers vectors $\boldsymbol{b} = a/2\langle 1\,1\,0\rangle$. The dislocation axes lie mainly along ⟨1 1 0⟩ and ⟨1 1 2⟩ directions. Sub-cell formation occurs in all instances and samples become polycrystalline after large strains of the order of 30%. The majority of sub-boundaries lay along ⟨1 1 0⟩ directions in the crystal and the density of dislocations in such boundaries was ~ 5 times greater than the overall crystal density. Dislocation estimates from etch pit and electron microscope techniques show good agreement in the range 10^5 to 10^8 cm^{-2}.

Acknowledgements

We are indebted to the Services Electronics Research Laboratories, and in particular to Mr P. Gurnell, for the supply of specimens and the construction of much of the apparatus. One of

us (D.L.) was in receipt of a grant from the Science Research Council.

References

1. J. R. PATEL and A. R. CHAUDHURI, *J. Appl. Phys.* **34** (1963) 2788.
2. R. L. BELL and W. BONFIELD, *Phil. Mag.* **9** (1964) 9.
3. A. STEINEMANN and U. ZIMMERLI, *Solid State Electron* **6** (1963) 597.
4. S. TIMOSHENKO and J. N. GOODIER, "Theory of Elasticity" (McGraw-Hill, New York, 1951).
5. A. A. BRUNEAU and P. L. PRATT, *Phil. Mag.* **7** (1962) 1871.
6. C. S. BARRETT, "Structure of Metals" (McGraw-Hill, New York and London, 1952).
7. J. R. PATEL and P. E. FREELAND, *J. Appl. Phys.* **38** (1967) 3087.
8. P. HAASEN and A. SEEGER, "Halbleiterprobleme" (Brauschweig-Vieweg, Berlin, 1958) **4** 68.
9. H. ALEXANDER, *Z. Metallk.* **52** (1961) 344.
10. A. R. CHAUDHURI, J. R. PATEL, and L. G. RUBIN, *J. Appl. Phys.* **33** (1962) 2736.
11. J. R. PATEL and A. R. CHAUDHURI, *ibid* **34** (1963) 2788.
12. J. R. LOW, JUN, and A. M. TURKALO, *Acta Metallurgica* **10** (1962) 215.
13. P. B. HIRSCH, A. HOWIE, R. B. NICHOLSON, D. W. PASHLEY, and M. J. WHELAN, "Electron Microscopy of Thin Films" (Butterworths, London, 1965).
14. A. HOWIE, "Direct Observation of Imperfections in Crystals", eds J. B. Newkirk and J. H. Wernick (Interscience, New York and London, 1962) p. 283.
15. J. HORNSTRA, *J. Phys. Chem. Solids* **5** (1958) 129.
16. W. G. JOHNSON and J. J. GILMAN, *J. Appl. Phys.* **30** (1959) 129.
17. A. H. COTTRELL, "Relationship between Structure and Mechanical Properties of Matter" (N.P.L. Symp., HMSO, 1963) p. 456.
18. N. P. SAZHIN, M. G. MIL'VIDSKII, V. B. OSVENSKII, and A. G. STOLYAROV, *Soc. Phys. Solid State* **8** (1966) 1223.
19. D. LAISTER and G. M. JENKINS, *Phil. Mag.* **23** (1971) 1077.
20. W. C. DASH, "Properties of Elemental and Compound Semiconductors", Met. Soc. Conf., Vol. **5**, Ed., H. C. Gatos (Interscience, New York and London, 1959).
21. V. CELLI, M. KABLER, T. NIMONIJA, and R. THOMPSON, *Phys. Rev.* **131** (1963) 58.
22. J. BLACK and P. LUBLIN, *J. Appl. Phys.* **35** (1964) 2467.
23. M. S. ABRAHAMS and L. EKSTROM, *Acta Metallurgica* **8** (1960) 654.
24. A. E. JENKINSON and A. R. LANG, "Direct Observation of Imperfections in Crystals" (Interscience, New York and London, 1962) p. 47.

Received 10 October and accepted 19 December 1972.